AIMS Mathematics, 10(4): 8965–8987.
DOI: 10.3934/math.2025411
Received: 29 January 2025
Revised: 23 March 2025
Accepted: 01 April 2025
Published: 18 April 2025

https://www.aimspress.com/journal/Math

Research article

Dynamics of Lie symmetry, Paul-Painlevé approach, bifurcation aalysis to the Ivancevic option pricing model via a optimal system of Lie subalgebra

Ibtehal Alazman*

Department of Mathematics and Statistics, College of Science, Imam Mohammad Ibn Saud Islamic University (IMSIU), Riyadh 13318, Saudi Arabia

* **Correspondence:** Email: iaazman@imamu.edu.sa.

Abstract: The Ivancevic model offers more accurate option pricing by including more grounded assumptions about the behavior of the market. Distinct forms of exact solutions are produced through the use of the analytical Paul-Painlevé method for the (1 + 1)-dimensional Ivancevic option pricing model. A five-dimensional Lie algebra is produced, with scaling and dilation as the remaining point symmetries in space and time. We employ symmetry reduction of Lie subalgebras to derive closed-form invariant solutions. In certain reduction cases, we convert the chosen model into a spectrum of non-linear ordinary differential equations (ODEs), which have the advantage of providing a large number of closed-form solitary wave solutions. Moreover, bifurcation theory is used to analyze planar dynamical systems at distinct equilibrium points, observing deviations under external perturbations and sensitivity under various initial conditions. Through these analyses, financial models can be made more robust by understanding how changes in model parameters or market conditions impact the dynamics and stability of option prices. These methods collectively enhance the understanding, robustness, and accuracy of option pricing models, providing valuable tools for both theoretical research and practical applications in nonlinear dynamics.

Keywords: Ivancevic option pricing model; Lie symmetry analysis; analytical approach; exact solution; qualitative analysis
Mathematics Subject Classification: 35A09, 35C08

1. Introduction

The economy and finance are very commonly studied subjects in the current era. Experts and scientists have manufactured many more advanced products by developing numerous technological and scientific instruments [1]. These tools are used to improve all aspects of daily living. At this point in the interaction between these gadgets and their users, the users need to know how to maximize the benefits

or obtain ideal values. Traditionally, when evaluating the worth of products, these users opt to rely on their existing knowledge. As a result, they encounter a variety of issues with buyers, sellers, banks, online platforms, local and global platforms, and more [2]. Thus, these issues have been researched and examined, utlilizing scientific standards. Consequently, keeping an eye on the financial market is crucial. Global informatics systems are produced by more detailed aspects of global financial market modelling. These dynamical systems in particular can be utilized to deeply examine the productions. The initial stage is to perform the mathematical models, which might be real or complex-valued with a wave function [3, 4].

In numerous scientific and technical domains, nonlinear partial differential equations (NLPDEs), are indispensable. Because they can more correctly explain complex systems and phenomena than linear equations, they are important. They are essential for both theoretical study and real-world applications because of their capacity to correctly represent real-world phenomena and capture nonlinear interactions. In order to address the complexities of dynamic and complex systems, NLPDEs offer the mathematical basis required, regardless of field such as physics, engineering, biology, or finance [5]. NLPDEs often exhibit many mathematical features, such as solitons and bifurcations, which are essential to understanding the underlying principles of many different kinds of phenomena. It aids in comprehending how modifications to parameters might result in qualitative changes in a system's behavior by highlighting crucial moments when the behaviour of the system drastically changes [6–8]. In addition to advancing interdisciplinary research and technological advancements, their work advances our comprehension of both natural and artificial systems. To analyze the behavior of complicated occurrences, one must be able to solve intricate mathematical models. A variety of efficient methods for obtaining precise solutions from NLPDEs have been developed by researchers over time. These methods include the following: the exponential rational function approach [9], the modified Jacobi elliptic expansion method [10], the inverse scattering method [11], the Hirota bilinear method [12], the Backlund transformation [13], the improved F-expansion method [14], the variational iteration method [15], and many other, [16–19].

The history of option pricing began in 1900 when French mathematician Louis Bachelier developed a formula based on the idea that stock prices follow free-drift Brownian motion. The idea of warrant and option pricing has since been the subject of several contributions from scholars and traders alike. A broad theory of contingent-claim pricing may result from an analysis of option pricing since the option is a specific kind of contingent-claim asset. A theoretical formula for option valuation, known as the Blacks-Scholes partial differential equation [20], was presented by Black and Scholes in 1973 after they noted that, if options are priced correctly, it is possible to profit by building portfolios of long and short positions in options and underlying assets.

$$\frac{\partial \Theta}{\partial t} + \sigma \Theta \frac{\partial \Theta}{\partial r} + \frac{\delta^2}{2} \Theta^2 \frac{\partial^2 \Theta}{\partial t^2} = \sigma \Theta, \tag{1.1}$$

where $\Theta = \Theta(r, t)$ is the market value of an option with stock price r and time t, defined in the domain $0 \leq r < \infty$, $0 \leq t \leq T$. σ is the risk-free interest rate, δ is the stock price volatility, and T is the maturity period.

Following the 2007 financial crisis, there has been a growing interest in using mathematical models that are different from the conventional methods. It is crucial to compare the Ivancevic model's efficacy to models like the Black-Scholes model, the Heston stochastic volatility model, and

the Jump-Diffusion model, even though it incorporates nonlinear dynamics that can capture intricate market patterns. Different strategies for managing volatility and abrupt market changes are incorporated into each of these models. For instance, the Black-Scholes model's simplicity and effectiveness may allow it to function well during times of low volatility. However, models that take into account stochastic volatility or nonlinear behavior, such as the Heston and Ivancevic models, may provide more accurate pricing in high-volatility or crisis situations, like those that occurred during the 2008 financial meltdown or the COVID-19 pandemic. The advantages of the Ivancevic model, such as its capacity to adjust to abrupt changes and identify pricing anomalies that conventional models frequently overlook, might be demonstrated by a comparison analysis utilizing historical option price data from different market regimes. Incorporating performance measurements like pricing bias, hedging efficiency, or root mean square error (RMSE) would offer a quantitative basis for evaluating the model's applicability. The inadequacy of classical stochasticity in characterizing financial progress became increasingly evident. In particular, many models that investigate the mathematical formalism of quantum mechanics have been created in order to provide insight into the financial market. Baaquie proposed in 1997 that the option price may be viewed as the quantum mechanical equivalent of the Schrödinger wave-function [21]. The option price was seen as a state function in 2002, and Haven [22] discovered a potential function that permits the option price to satisfy the Schrödinger equation, i.e.

$$V(r,t) = \frac{i\Re\Gamma + (\Re^2/2)\Xi}{G(r,t)}, \tag{1.2}$$

where $C(r,t)$ represents the call price, $\partial^2 C/\partial r^2$, and $\partial C/\partial t = \Gamma$. The Vanilla Black-Scholes solution fulfills the Schrödinger equation under the potential function mentioned above:

$$-\frac{\Re^2}{2m}\frac{\partial^2 C}{\partial r^2} + V(r,t)C(r,t) = i\Re\frac{\partial C}{\partial t}. \tag{1.3}$$

The Ivancevic model adds nonlinear dynamics and more realistic and adaptable modeling alternatives, particularly under volatile or extreme market settings, to conventional financial theory. Although the Black-Scholes model is more straightforward and popular, it is not as deep as the Ivancevic model, which attempts to capture phenomena like market shocks or chaos. Among the innovations in financial economics, the Ivancevic option pricing model is noteworthy. By integrating stochastic volatility and nonlinear dynamics, it overcomes the drawbacks of conventional models and offers an enhanced level of precision and comprehensiveness in option pricing. The model is extremely useful for both theoretical study and real-world applications because of its increased predictive capacity, adaptability, and integration of cutting-edge analytical approaches. The Ivancevic model is an important contribution to the development of financial modelling and economic theory since it enhances risk management, promotes regulatory compliance, and aids in strategic decision-making. Nonlinear dynamics are incorporated into the Ivancevic model, which explains complicated market behaviors such large tails, leaps, and volatility clustering. This results in financial market modelling that is more precise and realistic. Recently, Chen et al. [23] discussed the fundamental properties of the selected model by elaborating the tanh expansion technique and the trial function method. Jena et al. [24] analyse the core fractional characteristics of the selected model. Yan visualized the vector financial propagation of waves in [25]. Further, Edeki conducted an analysis on the non-zero adaptive market potential of the Ivancevic option pricing model in [26].

In order to create a complex-valued function that equals the probability density function for the value of a stock option, Vladimir G. Ivancevic [27] performed the quantum-probability construction and provided a nonlinear model. In this paper, we focus on the $(1+1)$-dimensional the Ivancevic option pricing model, which is mathematically formulated as [28]:

$$i\frac{\partial \Theta}{\partial t} + \frac{1}{2}\alpha\frac{\partial^2 \Theta}{\partial r^2} + \lambda|\Theta(r,t)|^2\Theta(r,t) = 0, \tag{1.4}$$

where $i = \sqrt{-1}$, $\Theta(r,t)$ is know as a function of complex-valued for r and t. Eq (1.4) uses r to describe the asset price of the product and defines $0 \leq r < 1$, whereas the independent variable t, which is $0 \leq t < T$, is used to represent time. To represent the option price wave function, we utilize the dependent variable $\Theta(r,t)$. Moreover, the potential field is indicated by the expression $|\Theta(r,t)|^2$, which also provides the probability density function. In addition, α, the dispersion frequency coefficient, represents the volatility as a constant or the stochastic process itself (it is treated as a constant in this study), and λ reflects the adaptive market potential. Comparing the option prices determined by the Ivancevic model with actual market prices offers a transparent, fact-based evaluation of the model's effectiveness in terms of option pricing accuracy. It is feasible to assess how closely the Ivancevic model resembles actual trading behavior by looking at price errors in both stable and dynamic markets. For instance, empirical research could calculate the absolute pricing error or mean squared error (MSE) between the outputs of the Black-Scholes and Ivancevic models in relation to actual market prices for frequently traded options, such as those listed on the Apple Inc. (AAPL) stock exchange. In addition to confirming the Ivancevic model's theoretical soundness, these comparisons show how useful it might be in high-volatility situations, where traditional models frequently fail.

The primary aim of this research is the encapsulation of the analysis of Lie symmetry, which could result in increased option pricing accuracy and predictability. The model's complicated differential equations are made simpler by the application of Lie symmetry analysis, which facilitates the identification of precise solutions and the comprehension of the underlying dynamics. The Paul-Painlevé methodology is used to identify benchmarks for option prices under certain conditions by identifying invariant solutions through symmetry methods. Additionally, the bifurcation analysis of the previously mentioned model is also analyzed. Numerous precise solutions that have not been reported in earlier literature have been produced by these studies. This is an extremely significant addition to risk management, as good decision-making requires accurate pricing estimations. By making graphs, we were also able to visually depict how the solutions behaved. The behavior of nonlinear systems that exhibit complicated and seemingly random motion due to their great sensitivity to beginning circumstances is referred to as chaotic dynamics [29]. Phase portraits and temporal evolution charts, where slight variations in parameters or initial conditions result in radically divergent trajectories, are used in our work to demonstrate chaotic dynamics. These characteristics demonstrate how chaotic systems in a regulated financial or physical environment are both deterministic and unexpected. Sensitivity analysis is a technique that examines how variations in a system's output are influenced by adjustments to its initial parameters or conditions. Because even slight variations in initial values can result in notable behavioral divergences over time, this approach is especially crucial in chaotic systems [30]. In our work, sensitivity analysis is carried out by comparing many system trajectories that begin with slightly varied initial values. The results demonstrate the instability and unpredictability characteristic of nonlinear dynamical systems, and prove the chaotic nature of the system by demonstrating a large divergence in its behavior.

The following is how the rest of our manuscript is organized: in Section 2, we present the description of the Paul-Painlevé approach. Section 3 describes the Lie symmetry analysis and symmetry reductions of the model. Section 4 describes the application of the Paul-Painlevé approach. Section 5 elaborates the bifurcation analysis of dynamical model. Section 6 signifies the sensitivity analysis of the model. In Section 7, the results are presented. We conclude our work in Section 8.

2. Description of the Paul-Painlevé approach

Nonlinear differential equations influence a wide variety of physical events. Understanding the qualitative behavior of solutions to these equations is made easier by the Painlevé technique, which is particularly useful in determining which solutions behave in a regular or chaotic manner.

Consider the non-linear partial differential equations

$$\mathfrak{I}(\Theta,\ \Theta_r,\ \Theta_t,\ \Theta_{rr},\ \Theta_{rrr}, \cdots) = 0. \tag{2.1}$$

Step-1. Assume the wave transformation as follows:

$$\Theta(r,t) = \varpi(\mathfrak{M}),\ \mathfrak{M}) = r + \gamma t. \tag{2.2}$$

Here, γ is the new independent variable for Eq (2.2). By plugging Eq (2.2) into Eq (2.1), we retrieve the following ODE:

$$Q(\varpi,\ \varpi',\ \varpi'', \cdots) = 0. \tag{2.3}$$

Step-2. Suppose the trial solution for Eq (2.3),

$$\varpi(\mathfrak{M}) = \sum_{i=1}^{m} \left[B_i \Omega^i(\aleph) e^{-in\mathfrak{M}} \right], \tag{2.4}$$

where the constants are B_i $(B_1,\ B_2, B_3,\ \cdots,\ B_M)$. The term $\Omega(\aleph)$ is fulfilled by the ODE $\frac{d\Omega}{d\aleph} - \kappa\Omega^2 = 0$, where $\aleph = \Re(\mathfrak{M}) = A_1 - \frac{e^{-n\mathfrak{M}}}{n}$ along with the results of Ricatti-equation given below:

$$\Omega(\aleph) = \frac{1}{\kappa\aleph - d_0}. \tag{2.5}$$

Step-3. From Eq (2.3), the value for m will be obtained by using the balancing technique, which states that the high degree of the nonlinear term balance the high order of derivatives.

Step-4. By inserting Eqs (2.4) and (2.5) into Eq (2.1), one may obtain the coefficients of the powers of $\Omega^i(\aleph)$, $(i = 0, 1, 2, 3, \cdots)$. After compiling the related terms equal to zero, we use the computer algebra system (CAS) Mathematica to solve a set of equations.

3. Analysis of Lie symmetry

The following assumption is made in order to differentiate between the imaginary and real parts of Eq (1.4):

$$\Theta(x,t) = \mathfrak{E}(r,t) + i\mathfrak{F}(r,t). \tag{3.1}$$

After substituting Eq (3.1) into Eq (1.4), the imaginary and real components are as follows:

$$-\mathfrak{F}_t + \lambda\mathfrak{E}\mathfrak{F}^2 + \lambda\mathfrak{E}^3 + \frac{1}{2}\alpha\mathfrak{E}_{rr} = 0, \tag{3.2}$$

$$\mathfrak{E}_t + \lambda\mathfrak{F}\mathfrak{E}^2 + \lambda\mathfrak{F}^3 + \frac{1}{2}\alpha\mathfrak{F}_{rr} = 0. \tag{3.3}$$

The symmetries of the studied Eq (1.4) are obtained by applying the Lie group method. For this, the following minuscule modifications are taken into account:

$$\begin{aligned} r^\star &= r + \epsilon\, \wp^1(r,t,\mathfrak{E},\mathfrak{F}) + \mathbb{O}(\epsilon^2),\\ t^\star &= t + \epsilon\, \wp^2(r,t,\mathfrak{E},\mathfrak{F}) + \mathbb{O}(\epsilon^2),\\ \mathfrak{E}^\star &= \mathfrak{E} + \epsilon\, \mathfrak{M}(r,t,\mathfrak{E},\mathfrak{F}) + \mathbb{O}(\epsilon^2),\\ \mathfrak{F}^\star &= \mathfrak{F} + \epsilon\, \mathfrak{N}(r,t,\mathfrak{E},\mathfrak{F}) + \mathbb{O}(\epsilon^2). \end{aligned} \tag{3.4}$$

The fluctuating ϵ indicates that the Lie group parameters are believed to be rather modest. Within the previously described transformation group's vector field, the transformation can be accessed.

$$\mathfrak{L} = \wp^1(r,t,\mathfrak{E},\mathfrak{F})\frac{\partial}{\partial r} + \wp^2(r,t,\mathfrak{E},\mathfrak{F})\frac{\partial}{\partial t} + \mathfrak{M}(r,t,\mathfrak{E},\mathfrak{F})\frac{\partial}{\partial \mathfrak{E}} + \mathfrak{N}(r,t,\mathfrak{E},\mathfrak{F})\frac{\partial}{\partial \mathfrak{F}}. \tag{3.5}$$

The coefficient functions $\wp^1(r,t,\mathfrak{E},\mathfrak{F})$, $\wp^2(r,t,\mathfrak{E},\mathfrak{F})$, $\mathfrak{M}(r,t,\mathfrak{E},\mathfrak{F})$, and $\mathfrak{N}(r,t,\mathfrak{E},\mathfrak{F})$ are to be determined, and the vector field $\mathfrak{L}$ satisfies the Lie symmetry condition if and only if

$$\mathbb{P}r^{[2]}\mathfrak{L}(\Delta_i)|_{\Delta_i=0} = 0, \quad i = 1, 2, \cdots \tag{3.6}$$

where $\Delta_1 = -\mathfrak{F}_t + \lambda\mathfrak{E}\mathfrak{F}^2 + \lambda\mathfrak{E}^3 + \frac{1}{2}\alpha\mathfrak{E}_{rr} = 0$ with prolongation expression

$$\mathfrak{L}^2 = \mathfrak{L} + \mathfrak{N}^t\frac{\partial}{\partial \mathfrak{F}_t} + \mathfrak{M}^{rr}\frac{\partial}{\partial \mathfrak{E}_{rr}}, \tag{3.7}$$

and $\Delta_2 = \mathfrak{E}_t + \lambda\mathfrak{F}\mathfrak{E}^2 + \lambda\mathfrak{F}^3 + \frac{1}{2}\alpha\mathfrak{F}_{rr} = 0$ with prolongation expression

$$\mathfrak{L}^2 = \mathfrak{L} + \mathfrak{M}^t\frac{\partial}{\partial \mathfrak{E}_t} + \mathfrak{N}^{rr}\frac{\partial}{\partial \mathfrak{F}_{rr}}, \tag{3.8}$$

along with,

$$\mathfrak{M}^i = D_i\Big[\mathfrak{M} - \sum_{l=1}^{2}\wp^l\mathfrak{E}_l^a\Big] + \sum_{l=1}^{2}\wp^l\mathfrak{E}_{i,l}^a, \tag{3.9}$$

$$\mathfrak{N}^i = D_i\Big[\mathfrak{N} - \sum_{l=1}^{2}\wp^l\mathfrak{F}_l^a\Big] + \sum_{l=1}^{2}\wp^l\mathfrak{F}_{i,l}^a, \text{ where } (1_1,\cdots,l_a),\ 1 < l_a \le 2,\ 1 \le a \le 2. \tag{3.10}$$

From these prolongations given in the preceding Eqs (3.7) and (3.8), we can deduce an algebra of Lie point symmetries by evaluating various derivatives of the dependent variable by their coefficients. These are calculated, and the generators that are listed are as follows:

$$\mathfrak{L}_1 = \frac{\partial}{\partial r}, \tag{3.11}$$

$$\mathfrak{L}_2 = \frac{\partial}{\partial t}, \tag{3.12}$$

$$\mathfrak{L}_3 = \mathfrak{F}\frac{\partial}{\partial \mathfrak{E}} - \mathfrak{E}\frac{\partial}{\partial \mathfrak{F}}, \tag{3.13}$$

$$\mathfrak{L}_4 = \alpha t\frac{\partial}{\partial r} - \mathfrak{F}r\frac{\partial}{\partial \mathfrak{E}} + \mathfrak{E}r\frac{\partial}{\partial \mathfrak{F}}, \tag{3.14}$$

$$\mathfrak{L}_5 = 2t\frac{\partial}{\partial t} - \mathfrak{F}\frac{\partial}{\partial \mathfrak{F}}\mathfrak{E}\frac{\partial}{\partial \mathfrak{E}} + r\frac{\partial}{\partial r}. \tag{3.15}$$

One must confirm that the symmetry Lie algebras of Eq (3.11) are generated by $\mathfrak{L}_i,\ i = 1, 2, 3, 4, 5$. We need to categorize these symmetry vector fields into groups that set them apart from one another since every combination of these vector fields is a symmetry algebra. All group invariant solutions require an ideal system concept to be explained.

3.1. Lie point groups

An infinite continuous group of transformations is obtained by implementing the set of infinitesimal vector fields $\mathfrak{L}_j,\ j \in 1, 2, \cdots, 5$ in Eq (3.11) on an infinite dimensional algebra. A suitable linear combination of $\mathfrak{L}$ can be used to illustrate the infinitesimal generator of Eq (3.11). The following are some cases of such combinations:

$$\mathfrak{C} = A_1\mathfrak{L}_1 + A_2\mathfrak{L}_2. \tag{3.16}$$

Lie symmetry analysis is used to study the invariance of equations via single parameter subgroups of set transformations whose infinitesimal generators are demonstrated as vector fields. The associated symmetry point algebras facilitate the computation of Lie symmetry groups and exact solutions for Eq (3.2) as well as Eq (3.3). By resolving the following equation, the Lie groups have been found:

$$\begin{aligned} \frac{d\hat{r}}{d\epsilon} &= \wp^1(\hat{r}, \hat{t}, \hat{\mathfrak{E}}, \hat{\mathfrak{F}}), \\ \hat{r}|_{\epsilon=0} &= r. \end{aligned}$$

$$\begin{aligned} \frac{d\hat{t}}{d\epsilon} &= \wp^2(\hat{r}, \hat{t}, \hat{\mathfrak{E}}, \hat{\mathfrak{F}}), \\ \hat{t}|_{\epsilon=0} &= t. \end{aligned}$$

$$\begin{aligned} \frac{d\hat{\mathfrak{E}}}{d\epsilon} &= \mathfrak{M}(\hat{r}, \hat{t}, \hat{\mathfrak{E}}, \hat{\mathfrak{F}}), \\ \hat{\mathfrak{E}}|_{\epsilon=0} &= \mathfrak{E}. \end{aligned}$$

$$\begin{aligned} \frac{d\hat{\mathfrak{F}}}{d\epsilon} &= \mathfrak{N}(\hat{r}, \hat{t}, \hat{\mathfrak{E}}, \hat{\mathfrak{F}}), \\ \hat{\mathfrak{F}}|_{\epsilon=0} &= \mathfrak{F}, \end{aligned}$$

where ϵ denotes the arbitrary parameter. Consequently,

$$\mathbb{H}_i\ : (r, t, \mathfrak{E}, \mathfrak{F}) \rightarrow\ (\hat{r}, \hat{t}, \hat{\mathfrak{E}}, \hat{\mathfrak{F}}). \tag{3.17}$$

3.2. The optimal system

The equivalence classes are obtained by splitting all of the invariant solutions of Eqs (3.2) and (3.3). When a Lie point symmetry transformation is used to differentiate between the two solutions, they are deemed equal. We require the selection of one unaltered solution from each equivalency class in order to build the entire class manipulating the symmetries of the system.

Definition 1. *A pair of Lie generators is said to be equal if they map to* $\mathfrak{L}$ *and* $\mathfrak{L}'$*. Categorizing invariant solutions corresponding to the symmetry generators of each result is crucial. One Lie generator per equivalence class can be selected to construct an optimal system. The following yields a Lie series:*

$$\mathfrak{U}\ \mathfrak{D}(exp(\epsilon\mathfrak{L}_i)\mathfrak{L}_j) = \mathfrak{L}_j - \epsilon[\mathfrak{L}_i, \mathfrak{L}_j] + \frac{\epsilon^2}{2}[\mathfrak{L}_i, [\mathfrak{L}_i, \mathfrak{L}_j]] - \cdots \tag{3.18}$$

The relations of the commutator $[\mathfrak{L}_i, \mathfrak{L}_j]$ *mention the combinedness of infinitesimal Lie generators (3.11) of the Ivancevic option pricing system (1.4). Specifically, the commutator* $[\mathfrak{L}_j, \mathfrak{L}_k]$ *and adjoint* $Adj[\epsilon\mathfrak{L}_j, \mathfrak{L}_k]$ *are provided in Tables 1 and 2. Assume a non-zero vector*

$$\mathfrak{L} = a\mathfrak{L}_1 + b\mathfrak{L}_2. \tag{3.19}$$

Our objective is to simplify the non-zero vector by employing efficient adjoint maps. Assuming $c \neq 0$*, we can employ* $a = 1$ *without losing generality:*

$$\mathfrak{L} = \mathfrak{L}_1 + b\mathfrak{L}_2. \tag{3.20}$$

The goal is to minimize the coefficients of the vector as much as possible. We utilize the terms of $\mathfrak{L}_2$ *once it has been extracted to investigate* $\mathfrak{L}$*. It is not immediately clear that the commutation relations being zero can further reduce the structure of the vector. Using the same process and standardizing the coefficients, we construct a one-dimensional optical system for subalgebras.*

$$\mathfrak{L}_1,\ \mathfrak{L}_2,\ \mathfrak{L}_3,\ \mathfrak{L}_1 + b\mathfrak{L}_2,\ \mathfrak{L}_1 + b\mathfrak{L}_2 + c\mathfrak{L}_3,$$

where b and c are arbitrary constant.

Table 1. The symmetry generator's commutator table for Eqs (3.2) and (3.3).

$[\mathfrak{L}_i, \mathfrak{L}_j]$	$\mathfrak{L}_1$	$\mathfrak{L}_2$	$\mathfrak{L}_3$	$\mathfrak{L}_4$	$\mathfrak{L}_5$
$\mathfrak{L}_1$	0	0	0	$-\alpha\mathfrak{L}_2$	$2\mathfrak{L}_1$
$\mathfrak{L}_2$	0	0	0	$\mathfrak{L}_3$	$\mathfrak{L}_2$
$\mathfrak{L}_3$	0	0	0	0	0
$\mathfrak{L}_4$	$\alpha\mathfrak{L}_2$	$-\mathfrak{L}_3$	0	0	$-\mathfrak{L}_4$
$\mathfrak{L}_5$	$-2\mathfrak{L}_1$	$-\mathfrak{L}_2$	0	$\mathfrak{L}_4$	0

Table 2. Table of adjoints for the symmetry generator of Eqs (3.2) and (3.3).

$\mathfrak{U}\ \mathfrak{D}(\exp(\epsilon\mathfrak{L}_i)\mathfrak{L}_j)$	$\mathfrak{L}_1$	$\mathfrak{L}_2$	$\mathfrak{L}_3$	$\mathfrak{L}_4$	$\mathfrak{L}_5$
$\mathfrak{L}_1$	$\mathfrak{L}_1$	$\mathfrak{L}_2$	$\mathfrak{L}_3$	$\alpha\epsilon\mathfrak{L}_2 + \mathfrak{L}_4$	$-2\epsilon\mathfrak{L}_1 + \mathfrak{L}_5$
$\mathfrak{L}_2$	$\mathfrak{L}_1$	$\mathfrak{L}_1$	$\mathfrak{L}_3$	$-\epsilon\mathfrak{L}_3 + \mathfrak{L}_4$	$-\epsilon\mathfrak{L}_2 + \mathfrak{L}_5$
$\mathfrak{L}_3$	$\mathfrak{L}_1$	$\mathfrak{L}_2$	$\mathfrak{L}_3$	$\mathfrak{L}_4$	$\mathfrak{L}_5$
$\mathfrak{L}_4$	$-\alpha\epsilon\mathfrak{L}_2 + \mathfrak{L}_1 - \frac{1}{2}\alpha\epsilon^2\mathfrak{L}_3$	$\mathfrak{L}_2 + \epsilon\mathfrak{L}_3$	$\mathfrak{L}_3$	$\mathfrak{L}_4$	$\epsilon\mathfrak{L}_4 + \mathfrak{L}_5$
$\mathfrak{L}_5$	$e^{2\epsilon}\mathfrak{L}_1$	$e^{\epsilon}\mathfrak{L}_2$	$\mathfrak{L}_3$	$e^{-\epsilon}\mathfrak{L}_4$	$\mathfrak{L}_5$

3.3. Symmetry reduction to the Ivancevic option pricing model Eqs (3.2) and (3.3)

This section uses symmetry generators to calculate the symmetry reduction and then extracts the precise solution for the scenarios that are covered below.

3.3.1. $\mathfrak{T}_1 = \langle \mathfrak{Q}_1 \rangle = \frac{\partial}{\partial r}$

Hence, the Lagrange equation is represented as,

$$\frac{dr}{1} = \frac{dt}{0} = \frac{d\mathfrak{E}}{0} = \frac{d\mathfrak{F}}{0}. \tag{3.21}$$

From the solution of the previously given characteristic equation Eq (3.21), we obtain

$$\mathfrak{E} = P[\mathfrak{M}], \quad \mathfrak{F} = Q[\mathfrak{M}], \tag{3.22}$$

with $\mathfrak{M} = t$. By using Eq (3.22) in Eqs (3.2) and (3.3), we retrieve,

$$-Q' + \lambda PQ^2 + \lambda P^3 = 0, \tag{3.23}$$

$$P' + \lambda QP^2 + \lambda Q^3 = 0. \tag{3.24}$$

3.3.2. $\mathfrak{T}_2 = \langle \mathfrak{Q}_2 \rangle = \frac{\partial}{\partial t}$

Hence, the Lagrange equation is represented as

$$\frac{dr}{0} = \frac{dt}{1} = \frac{d\mathfrak{E}}{0} = \frac{d\mathfrak{F}}{0}. \tag{3.25}$$

From the solution of the previously given characteristic equation Eq (3.25) the following defined variables are obtained:

$$\mathfrak{E} = P[\mathfrak{M}], \quad \mathfrak{F} = Q[\mathfrak{M}], \tag{3.26}$$

with $\mathfrak{M} = r$. Using Eq (3.26) in Eqs (3.2) and (3.3), we obtain the following ODEs:

$$\frac{1}{2}\alpha Q'' + \lambda PQ^2 + \lambda P^3 = 0, \frac{1}{2}\alpha P'' + \lambda QP^2 + \lambda Q^3 = 0. \tag{3.27}$$

3.3.3. $\mathfrak{T}_3 = \langle \mathfrak{Q}_3 \rangle = \mathfrak{F}\frac{\partial}{\partial \mathfrak{E}} - \mathfrak{E}\frac{\partial}{\partial \mathfrak{F}}$

Hence, the Lagrange equation is illustrated as

$$\frac{dr}{0} = \frac{dt}{0} = \frac{d\mathfrak{E}}{\mathfrak{F}} = \frac{d\mathfrak{F}}{-\mathfrak{E}}. \tag{3.28}$$

The solution of the previously given characteristic equation Eq (3.28) yields

$$\mathfrak{E} = -P[\zeta]\cos[\mathfrak{N}] + Q[\zeta]\sin[\mathfrak{N}], \quad \mathfrak{F} = -P[\zeta]\sin[\mathfrak{N}] - Q[\zeta]\cos[\mathfrak{N}], \tag{3.29}$$

with $\zeta = \zeta(\mathfrak{M}, \mathfrak{N})$, where $\mathfrak{M} = x$ and $\mathfrak{N} = t$. Putting Eq (3.29) in Eqs (3.2) and (3.3), we derive

$$P + \frac{1}{2}\alpha Q'' + \lambda PQ^2 + \lambda P^3 = 0, \tag{3.30}$$

$$Q + \frac{1}{2}\alpha P'' + \lambda QP^2 + \lambda Q^3 = 0. \tag{3.31}$$

3.3.4. $\mathfrak{T}_4 = \langle \mathfrak{Q}_4 \rangle = \alpha t \frac{\partial}{\partial r} - \mathfrak{F} r \frac{\partial}{\partial \mathfrak{E}} + \mathfrak{E} r \frac{\partial}{\partial \mathfrak{F}}$

Hence, the Lagrange equation is represented as,

$$\frac{dr}{\alpha t} = \frac{dt}{0} = \frac{d\mathfrak{E}}{-r\mathfrak{F}} = \frac{d\mathfrak{F}}{r\mathfrak{E}}. \tag{3.32}$$

From the solution of the previously given characteristic equation Eq. (3.32), we get

$$\mathfrak{E} = -P[\mathfrak{M}] \cos[\frac{r}{\gamma}] + Q[\mathfrak{M}] \sin[\frac{r}{\gamma}], \quad \mathfrak{F} = P[\mathfrak{M}] \cos[\frac{r}{\gamma}] + Q[\mathfrak{M}] \sin[\frac{r}{\gamma}], \tag{3.33}$$

with $\mathfrak{M} = t$. Plugging Eq (3.33) in Eqs (3.2) and (3.3), we obtain

$$P + \frac{1}{2}\alpha Q'' + \lambda P Q^2 + \lambda P^3 = 0, \tag{3.34}$$

$$-Q + \frac{1}{2}\alpha P'' + \lambda Q P^2 + \lambda Q^3 = 0. \tag{3.35}$$

3.3.5. $\mathfrak{T}_5 = \langle \mathfrak{Q}_1 + \gamma \mathfrak{Q}_2 \rangle$

Hence, the Lagrange equation is represented as

$$\frac{dr}{1} = \frac{dt}{\gamma} = \frac{d\mathfrak{E}}{0} = \frac{d\mathfrak{F}}{0}. \tag{3.36}$$

From the solution of the previously given characteristic equation Eq (3.36), we obtain

$$\mathfrak{E} = P[\mathfrak{M}], \quad \mathfrak{F} = Q[\mathfrak{M}], \tag{3.37}$$

with $\mathfrak{M} = r - \gamma t$. Substituting Eq (3.37) into Eqs (3.2) and (3.3), we obtain

$$\gamma P' + \frac{1}{2}\alpha Q'' + \lambda P Q^2 + \lambda P^3 = 0, \tag{3.38}$$

$$-\gamma Q' + \frac{1}{2}\alpha P'' + \lambda Q P^2 + \lambda Q^3 = 0. \tag{3.39}$$

3.3.6. $\mathfrak{T}_6 = \langle \mathfrak{Q}_1 + \gamma \mathfrak{Q}_3 \rangle$

Hence, the Lagrange equation is represented as

$$\frac{dr}{1} = \frac{dt}{0} = \frac{d\mathfrak{E}}{-\gamma\mathfrak{F}} = \frac{d\mathfrak{F}}{\gamma\mathfrak{E}}. \tag{3.40}$$

From the solution of the previously given characteristic Eq. (3.40), we obtain

$$\mathfrak{E} = -P[\mathfrak{M}] \cos[\frac{r}{\gamma}] + Q[\mathfrak{M}] \sin[\frac{r}{\gamma}], \quad \mathfrak{F} = -P[\mathfrak{M}] \sin[\frac{r}{\gamma}] - Q[\mathfrak{M}] \cos[\frac{r}{\gamma}], \tag{3.41}$$

with $\mathfrak{M} = \gamma t$. Using Eq (3.41) in Eqs (3.2) and (3.3), we extract the following ODEs:

$$\gamma P + \frac{1}{2}\alpha Q'' + \lambda P Q^2 + \lambda P^3 = 0, \tag{3.42}$$

$$-\gamma Q + \frac{1}{2}\alpha P'' + \lambda Q P^2 + \lambda Q^3 = 0. \tag{3.43}$$

4. Construction of exact solutions of the Ivancevic option pricing model

By using the acquired Lie point symmetries, the examined partial differential equation (PDE) Eq (1.4) has been converted into distinct ODEs. A Paul-Painlevé scheme is applied to derive precise solutions for the non-linear Ivancevic option pricing model.

4.1. Paul-Painlevé scheme to Eq (3.30)

To obtain the invariant results for the Ivancevic option pricing, assume Eq (3.30). Setting $Q = \mu P$, Eq (3.30) can be represented as follows:

$$P + \frac{1}{2}\mu\alpha P'' + 2\mu^2\lambda P^3 = 0. \tag{4.1}$$

By using the homogeneous balancing theory, we obtain

$$P = B_0 + B_1\Omega(\aleph)e^{-n\mathfrak{M}}, \tag{4.2}$$

After plugging solution (4.2) into Eq (4.1), the system of algebraic equation is obtained by gathering coefficients that are unique powers of $\Omega(\aleph)$. Using Mathematica, the obtained system is solved, and the solution set is obtained follows:

Family-1:

$$a_0 = -\frac{i}{\sqrt{2}\sqrt{\lambda}\sqrt{\mu}},\ a_1 = \frac{i\sqrt{2}\kappa}{\sqrt{\lambda}\sqrt{\mu}n},\ \alpha = \frac{4}{\mu n^2}. \tag{4.3}$$

This yields

$$P(\mathfrak{M}) = -\frac{i\left(1 - \frac{2\kappa e^{\eta(-n)}}{\kappa n\aleph - d_0 n}\right)}{\sqrt{2}\sqrt{\lambda}\sqrt{\mu}},\ Q(\mathfrak{M}) = -\mu\frac{i\left(1 - \frac{2\kappa e^{\eta(-n)}}{\kappa n\aleph - d_0 n}\right)}{\sqrt{2}\sqrt{\lambda}\sqrt{\mu}}. \tag{4.4}$$

Using the above solutions of $P(\mathfrak{M})$ and $Q(\mathfrak{M})$ in Eq (3.29) yields:

$$\Theta_{1,1}(r,t) = \frac{(\mu - i)e^{\eta(-n)}(\cos(t) + i\sin(t))\left(d_0 n e^{\eta n} + 2\kappa - \kappa n\aleph e^{\eta n}\right)}{\sqrt{2}\sqrt{\lambda}\sqrt{\mu}n\left(\kappa\aleph - d_0\right)}. \tag{4.5}$$

Family-2:

$$a_0 = \frac{i}{\sqrt{2}\sqrt{\lambda}\sqrt{\mu}},\ a_1 = a_1,\ n = \frac{2}{\sqrt{\alpha}\sqrt{\mu}},\ \kappa = \frac{i\sqrt{2}a_1\sqrt{\lambda}}{\sqrt{\alpha}}. \tag{4.6}$$

This yields

$$P(\mathfrak{M}) = \frac{a_1 e^{-\frac{2\eta}{\sqrt{\alpha}\sqrt{\mu}}}}{-d_0 + \frac{i\sqrt{2}a_1\sqrt{\lambda}\aleph}{\sqrt{\alpha}}} + \frac{i}{\sqrt{2}\sqrt{\lambda}\sqrt{\mu}},\ Q(\mathfrak{M}) = \mu\left(\frac{a_1 e^{-\frac{2\eta}{\sqrt{\alpha}\sqrt{\mu}}}}{-d_0 + \frac{i\sqrt{2}a_1\sqrt{\lambda}\aleph}{\sqrt{\alpha}}} + \frac{i}{\sqrt{2}\sqrt{\lambda}\sqrt{\mu}}\right). \tag{4.7}$$

Using the above solutions of $P(\mathfrak{M})$ and $Q(\mathfrak{M})$ in Eq (3.29), we extract the solution of Eq (1.4):

$$\Theta_{1,2}(r,t) = \frac{\left(\frac{1}{2} - \frac{i}{2}\right)e^{-\frac{2\eta}{\sqrt{\alpha}\sqrt{\mu}}}(\cos(t) + i\sin(t))\left(-2a_1\sqrt{\lambda}\left(\sqrt{\alpha}\sqrt{\mu} - \aleph e^{\frac{2\eta}{\sqrt{\alpha}\sqrt{\mu}}}\right) + i\sqrt{2}\sqrt{\alpha}d_0 e^{\frac{2\eta}{\sqrt{\alpha}\sqrt{\mu}}}\right)}{\sqrt{\lambda}\sqrt{\mu}\left(\sqrt{2}a_1\sqrt{\lambda}\aleph + i\sqrt{\alpha}d_0\right)}. \tag{4.8}$$

4.2. Paul-Painlevé scheme to Eq (3.34)

To obtain the invariant results for the Ivancevic option pricing, assume Eq (3.34). Setting $Q = \mu P$, Eq (3.34) can be represented as follows:

$$P + \frac{1}{2}\mu\alpha P'' + 2\mu^2\lambda P^3 = 0. \tag{4.9}$$

By elaborating the homogeneous balancing rule, we get,

$$P = B_0 + B_1\Omega(\aleph)e^{-n\mathfrak{M}}. \tag{4.10}$$

After plugging solution (4.10) into equation (4.9), the system of algebraic equation is obtained by gathering coefficients that are unique powers of $\Omega(\aleph)$. Using Mathematica, the obtained system is solved, and the solution set is obtained as follows:

Family-3:

$$a_0 = a_0,\ a_1 = \sqrt{\alpha}a_0(-\kappa)\sqrt{\mu},\ n = \frac{2}{\sqrt{\alpha}\sqrt{\mu}},\ \lambda = -\frac{1}{2a_0^2\mu}. \tag{4.11}$$

This yields

$$P(\mathfrak{M}) = -(a_0\left(1 - \frac{\sqrt{\alpha}\kappa\sqrt{\mu}e^{-\frac{2\eta}{\sqrt{\alpha}\sqrt{\mu}}}}{\kappa\aleph - d_0}\right),\ Q(\mathfrak{M}) = \mu(a_0\left(1 - \frac{\sqrt{\alpha}\kappa\sqrt{\mu}e^{-\frac{2\eta}{\sqrt{\alpha}\sqrt{\mu}}}}{\kappa\aleph - d_0}\right). \tag{4.12}$$

Using the above solutions of $P(\mathfrak{M})$ and $Q(\mathfrak{M})$ in Eq (3.33), we retrieve the following solution of Eq (1.4):

$$\Theta_{1,3}(r,t) = \frac{(1-i)a_0e^{-\frac{2\eta}{\sqrt{\alpha}\sqrt{\mu}}}\left(\cos\left(\frac{r}{\gamma}\right) - i\mu\sin\left(\frac{r}{\gamma}\right)\right)\left(\kappa\aleph\left(-e^{\frac{2\eta}{\sqrt{\alpha}\sqrt{\mu}}}\right) + d_0e^{\frac{2\eta}{\sqrt{\alpha}\sqrt{\mu}}} + \sqrt{\alpha}\kappa\sqrt{\mu}\right)}{\kappa\aleph - d_0}. \tag{4.13}$$

4.3. Paul-Painlevé scheme to Eq (3.42)

To obtain the invariant solution of the Ivancevic option pricing, assume Eq (3.42). Setting $Q = \mu P$, Eq (3.42) can be represented as follows:

$$P + \frac{1}{2}\mu\alpha P'' + 2\mu^2\lambda P^3 = 0. \tag{4.14}$$

By establishing the homogeneous balancing principle, we obtain

$$P = B_0 + B_1\Omega(\aleph)e^{-n\mathfrak{M}}, \tag{4.15}$$

After plugging solution (4.15) into equation (4.14), the system of algebraic equation is obtained by gathering coefficients that are unique powers of $\Omega(\aleph)$. Using Mathematica, the obtained system is solved, and the solution set is obtained as follows:

Family-4:

$$a_0 = -\frac{\sqrt{-\frac{i(\sqrt{3}-i)\alpha n^2}{\lambda}}}{2\sqrt{3}},\ a_1 = \frac{i\kappa\lambda\left(-\frac{i(\sqrt{3}-i)\alpha n^2}{\lambda}\right)^{3/2}}{4\alpha n^3},\ \gamma = \frac{1}{2}i\sqrt{3}\alpha n. \tag{4.16}$$

This yields

$$P(\mathfrak{M}) = (\frac{1}{12}\sqrt{-\frac{i\left(\sqrt{3}-i\right)\alpha n^2}{\lambda}}\left(-2\sqrt{3}+\frac{3\left(\sqrt{3}-i\right)\kappa e^{\eta(-n)}}{n\left(\kappa\aleph-d_0\right)}\right),$$
$$Q(\mathfrak{M}) = \mu(\frac{1}{12}\sqrt{-\frac{i\left(\sqrt{3}-i\right)\alpha n^2}{\lambda}}\left(-2\sqrt{3}+\frac{3\left(\sqrt{3}-i\right)\kappa e^{\eta(-n)}}{n\left(\kappa\aleph-d_0\right)}\right). \tag{4.17}$$

Using above solutions of $P(\mathfrak{M})$ and $Q(\mathfrak{M})$ in Eq (3.41), we retrieve the solution of Eq (1.4):
Family-4:

$$\Theta_{1,4}(r,t) = \frac{(\mu-i)e^{\eta(-n)}\sqrt{-\frac{i\left(\sqrt{3}-i\right)\alpha n^2}{\lambda}}\left(2i\sqrt{3}d_0 ne^{\eta n}+\kappa\left(-2i\sqrt{3}n\aleph e^{\eta n}+3i\sqrt{3}+3\right)\right)}{12n\left(\kappa\aleph-d_0\right)}. \tag{4.18}$$

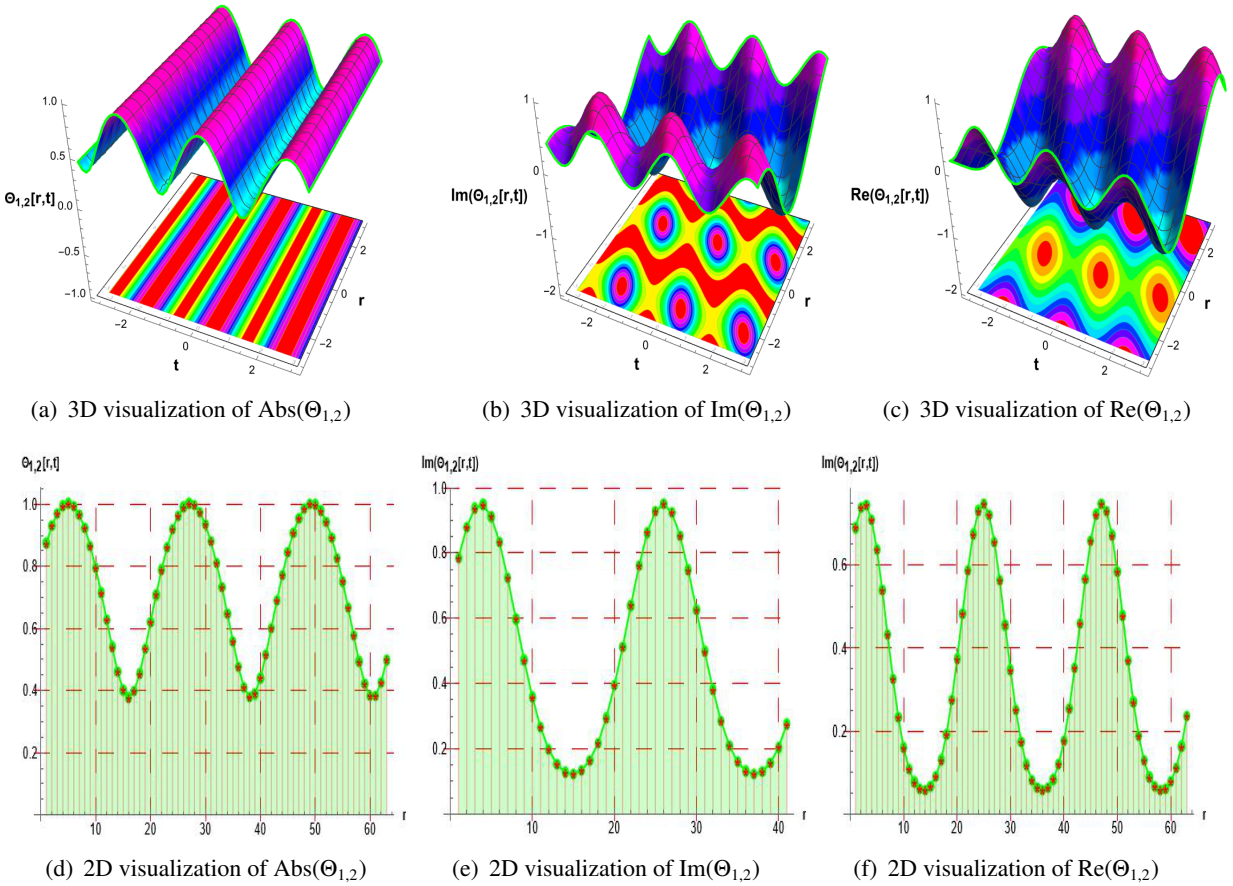

(a) 3D visualization of Abs($\Theta_{1,2}$) (b) 3D visualization of Im($\Theta_{1,2}$) (c) 3D visualization of Re($\Theta_{1,2}$)

(d) 2D visualization of Abs($\Theta_{1,2}$) (e) 2D visualization of Im($\Theta_{1,2}$) (f) 2D visualization of Re($\Theta_{1,2}$)

Figure 1. The distinct graphical behavior of the invariant solution for the solution $\Theta_{1,2}(r,t)$ which is demonstrated by setting the appropriate parameters $\mu = -1,\ \lambda = 2.1,\ n = 3.45,\ \aleph = 1.4,\ d_0 = -0.8,\ \alpha = 0.5,\ and\ a_1 = 0.4$.

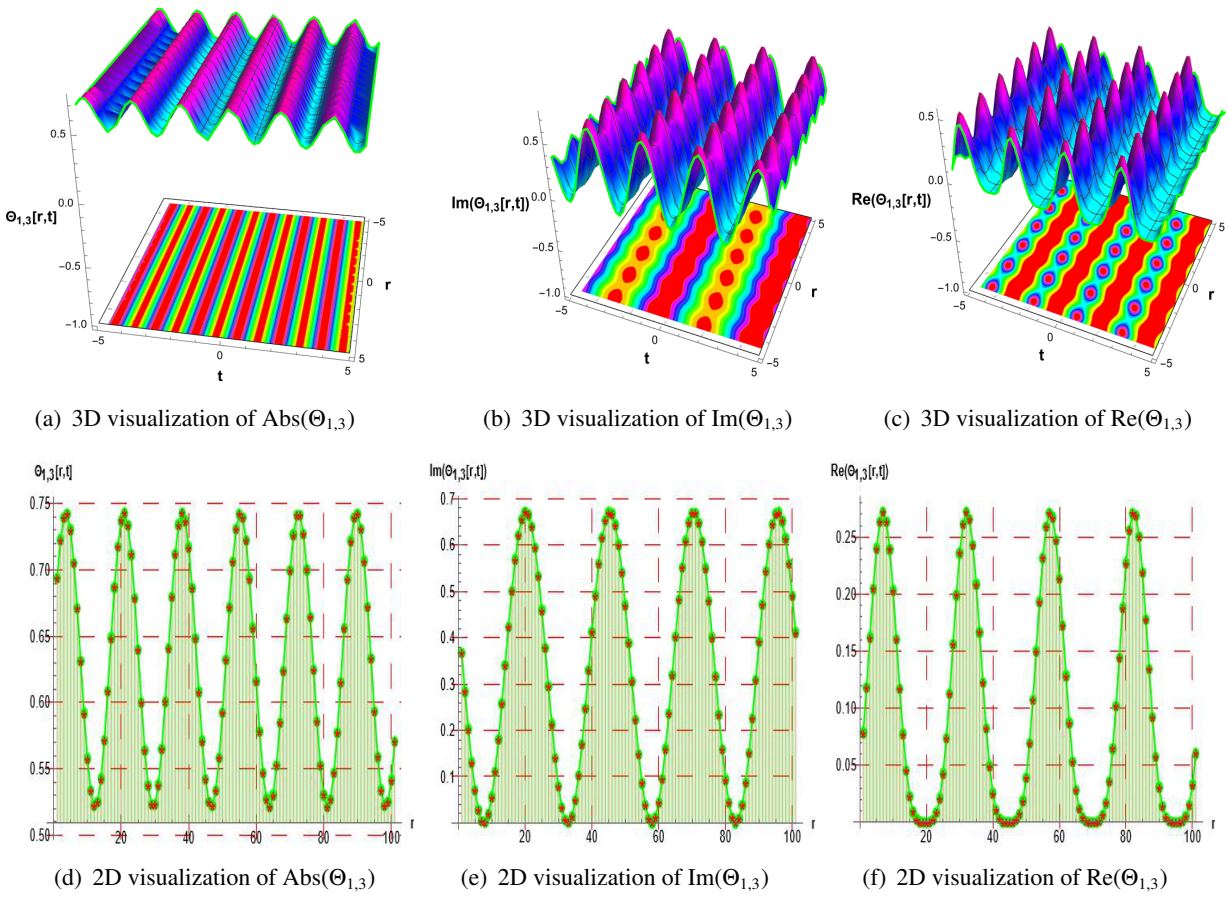

(a) 3D visualization of Abs($\Theta_{1,3}$) (b) 3D visualization of Im($\Theta_{1,3}$) (c) 3D visualization of Re($\Theta_{1,3}$)

(d) 2D visualization of Abs($\Theta_{1,3}$) (e) 2D visualization of Im($\Theta_{1,3}$) (f) 2D visualization of Re($\Theta_{1,3}$)

Figure 2. The distinct graphical behavior of the invariant solution for the solution $\Theta_{1,3}(r,t)$, which is demonstrated by setting the appropriate parameters $\eta = t$, $\mu = -1$, $n = 3$, $k = 0.5$, $\aleph = 0.94$, $d_0 = -1$, $\kappa = 0.19$, $\alpha = 0.3$, $\gamma = 0.8$, *and* $a_0 = 0.56$.

5. Analysis of bifurcation

To leverage the dynamic behavior of the analyzed model, we apply the following transformations:

$$\frac{d^m P}{d\mathfrak{M}^m} = (-1)^m \frac{d^m Q}{d\mathfrak{M}^m}, \quad P^m = Q^m. \tag{5.1}$$

The single ODE can be obtained from the coupled one in Eq (3.42) as

$$\gamma Q + \frac{1}{2}\alpha Q'' + 2\lambda Q^3 = 0. \tag{5.2}$$

Here, we examine the system's bifurcation, including the analysis of phase portraits for the system described by Eq (5.2). The significance of bifurcation analysis [31] lies in its ability to provide insights into qualitative changes in system behavior, identify crucial parameters, guarantee stability, forecast chaos, optimize system design, and investigate complicated dynamics in a variety of domains. Better insights, ideas, and policies can be achieved by using its potent instrument for dynamic system analysis

and control. We will resolve the following differential equations of dynamic systems presented below:

$$\begin{cases} \frac{dG}{d\mathfrak{M}} = W(\mathfrak{M}) = S_1, \\ \frac{dW}{d\mathfrak{M}} = -\vartheta_1 W(\mathfrak{M}) - \vartheta_2 W^3(\mathfrak{M}) = S_2. \end{cases} \tag{5.3}$$

Here, $\vartheta_1 = \frac{2\gamma}{\alpha}$ and $\vartheta_2 = \frac{4\lambda}{\alpha}$. Equation (5.3) has the following equilibrium points (EPs):

$$g_1 = (0, 0), \qquad g_2 = (\sqrt{-\frac{\vartheta_1}{\vartheta_2}}, 0), \qquad g_3 = (-\sqrt{-\frac{\vartheta_1}{\vartheta_2}}, 0).$$

The Jacobian (5.3) gives

$$\mathbb{J}(G, W) = \begin{vmatrix} 0 & 1 \\ -\vartheta_1 - 3\vartheta_2 W^2(\mathfrak{M}) & 0 \end{vmatrix} = -\vartheta_1 - 3\vartheta_2 W^2(\mathfrak{M}). \tag{5.4}$$

Hence,

• (G,0) gives saddle points when $\mathbb{J}(G, W) < 0$,

• (G,0) gives center points when $\mathbb{J}(G, W) > 0$,

• (G,0) gives cuspidal points when $\mathbb{J}(G, W) = 0$.

Below is a description of the possible results that can be obtained by changing the settings.

• **Case-(i)** When $\vartheta_1 < 0$ & $\vartheta_2 > 0$, under the specific parameters $\alpha = 0.3$, $\lambda = 4$, *and* $\gamma = -8$, we identify EP: $h_1 = (0, 0)$, $h_2 = (1, 0)$, $h_3 = (-1, 0)$. A visual representation of this can be seen in Figure 3, where h_2, and h_3 represent center-like positions, and h_1 depicts saddle behavior.

• **Case-(ii)** When $\vartheta_1 < 0$ & $\vartheta_2 < 0$, under the specific parameters $\alpha = -0.1$, $\lambda = 1$, and $\gamma = 3.4$, we identified the EPs, $h_1 = (i, 0)$, and $h_2 = (-i, 0)$, which are plotted in Figure 4, where h_1 refers to the cusp point, while the remaining two illustrate the saddle points.

• **Case-(iii)** When $\vartheta_1 > 0$ and $\vartheta_2 > 0$, under the specific parameters, $\alpha = 0.3$, $\lambda = 4$, and $\gamma = 8$, we identified three EPs. $h_1 = (0, 0)$, $h_2 = (-i, 0)$, and $h_3 = (i, 0)$. These EPs are represented in Figure 5, which shows the phase portrait. Here, h_1 demonstrates a center-like structure, whereas h_2, and h_3 demonstrate saddle points.

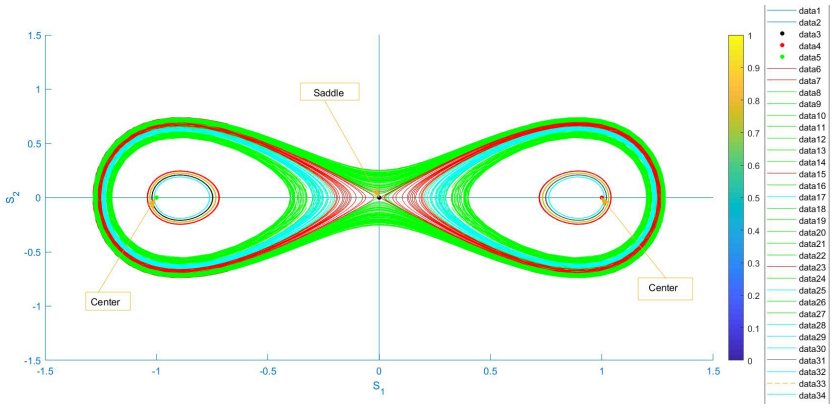

(a)

Figure 3. Phase variation plots of case (i).

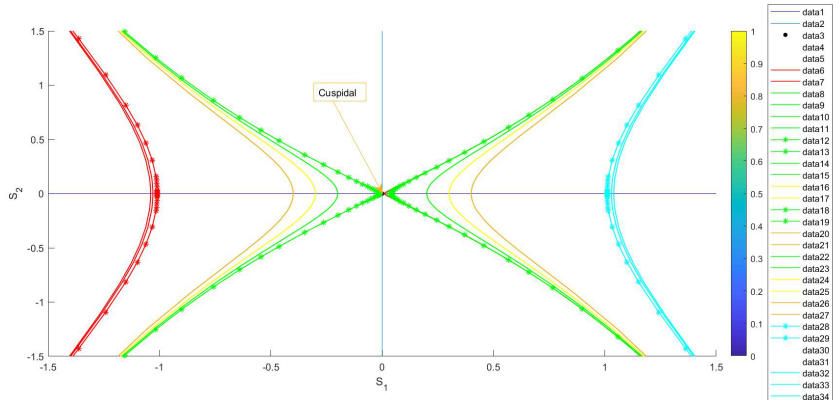

(a)

Figure 4. Phase variation plots of case (ii).

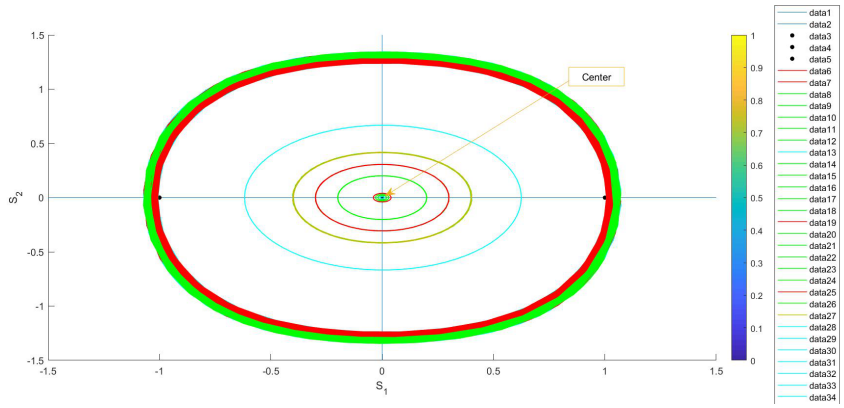

(a)

Figure 5. Phase variation plots of case (iii).

Bifurcation analysis and phase portraiture are essential techniques for managing, understanding, and depicting the behavior of dynamical systems. By graphing the state variables of a dynamical system against one another in a phase space, a phase portrait provides a potent visual aid for analyzing the behavior of the system. Their ability to clarify complex behaviors, stability, and system transitions makes them indispensable tools for both theoretical research and practical applications across numerous industries.

Here, analysis and examples of the possible formation of chaos in the system given in Eq (5.3) including perturbation are. Further, we analyze both two and three-dimensional plots for the system under consideration. After utilizing the perturbation term, we obtain

$$\begin{cases} \frac{dG}{d\mathfrak{M}} = W(\mathfrak{M}), \\ \frac{dW}{d\mathfrak{M}} = -\varpi_1 G(\mathfrak{M}) - \varpi_2 G^3(\mathfrak{M}) + \Upsilon_1 \cos(\Upsilon_2 t). \end{cases} \tag{5.5}$$

In order to analyze the system, the 2D and 3D time phase diagrams are exhibited using the values as $\gamma_1 = 2.5,\ \alpha = 0.9,\ \lambda = 0.3$. For this, two different sets of values are considered as: $[(a), (b)]\ \Upsilon_1 = 2.5,$

$\Upsilon_2 = 3.91$, and $[(c),(d)]$ $\Upsilon_1 = 4.1$, $\Upsilon_2 = 4.91$, as demonstrated in Figure 6. Furthermore, in Figure 7, we display different types of frequency and amplitude values: $[(a),(b)]$ $\Upsilon_1 = 1.2$, $\Upsilon_2 = -3.4$, and $[(c),(d)]$ $\Upsilon_1 = 1.5$, $\Upsilon_2 = 4.2$, as shown in Figure 7. The phase picture analysis reveals highly complex and fascinating dynamics, showing how the behavior of the suggested system is vulnerable to disturbances that arise in Υ_2. Additionally, it offers crucial information about the effects of the perturbation term $\Upsilon_1 cos(\Upsilon_2 t)$ on the behavior of the system. Our comprehension of the complex connections between Υ_2 and the overall dynamics of the system is enhanced by these fresh revelations regarding the system's vulnerability to parameter changes. These revelations successfully advance a more thorough understanding of how often minor changes could change the trajectory of the proposed dynamical system, ultimately leading to more accurate and informed forecasts of its actions in different scenarios.

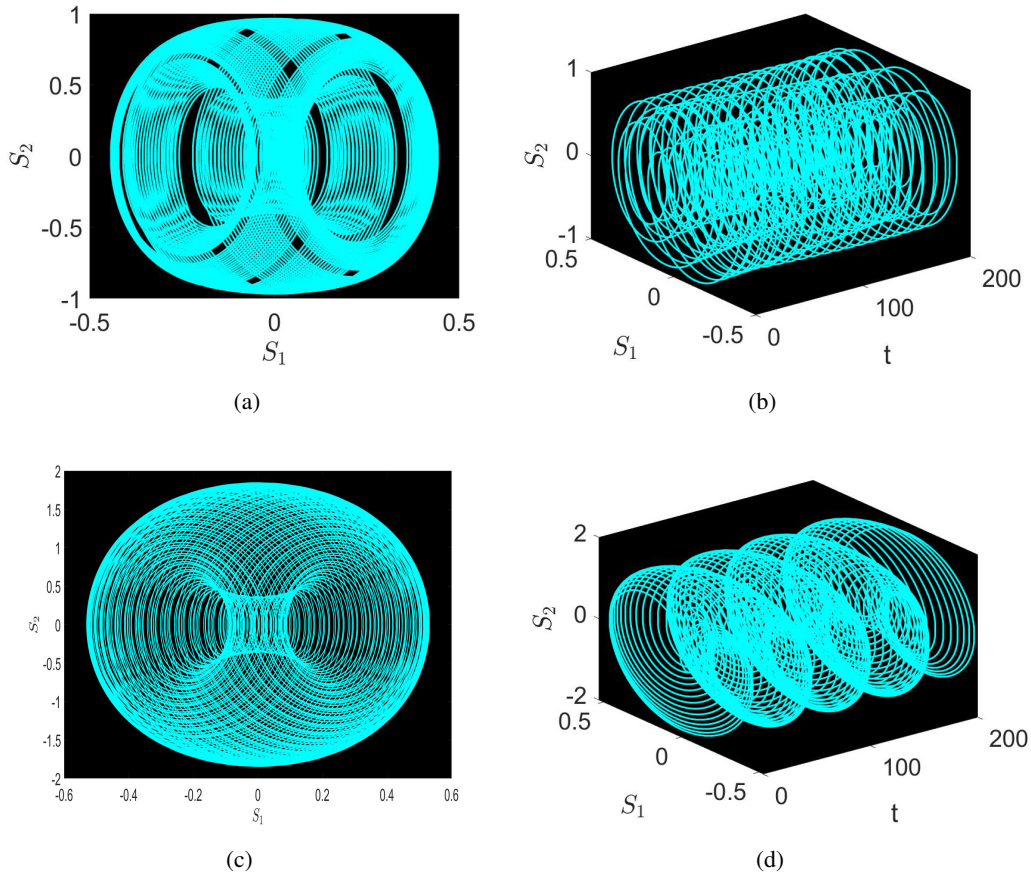

Figure 6. Using random parametric parameters, the system chaotic behavior in two and three dimensions is physically visualized (5.3).

The subplot (6(a)–6(b)) represents the trajectory in the S_1, S_2 plane. The trajectories are tightly packed and non-repeating, indicating chaotic or quasi-periodic motion and emphasizing how sensitive the system is to initial conditions. The subplot (6(c)–6(d)) shows a similar behavior but with a significantly larger amplitude in the direction of the S_2 plane and a denser trajectory pattern. This implies a shift to a more chaotic state, most likely brought on by more nonlinearity, increased external forcing, or increased system energy. The trajectory in the subplot (7(a)–7(b)) fills the phase space in a

symmetrical, butterfly-like pattern of curves. The motion in this complex pattern is aperiodic and extremely sensitive to initial conditions, indicating a somewhat chaotic regime. The subplot (7(c)–7(d)) displays a less congested and more ordered phase portrait. While retaining the characteristic symmetry, the trajectories form smooth, regularly spaced loops that indicate lesser chaos or near-periodic structure. When combined, these graphs highlight how many dynamical behaviors within the same system can result from changes in initial conditions or external stimulus, demonstrating the variety in chaotic systems.

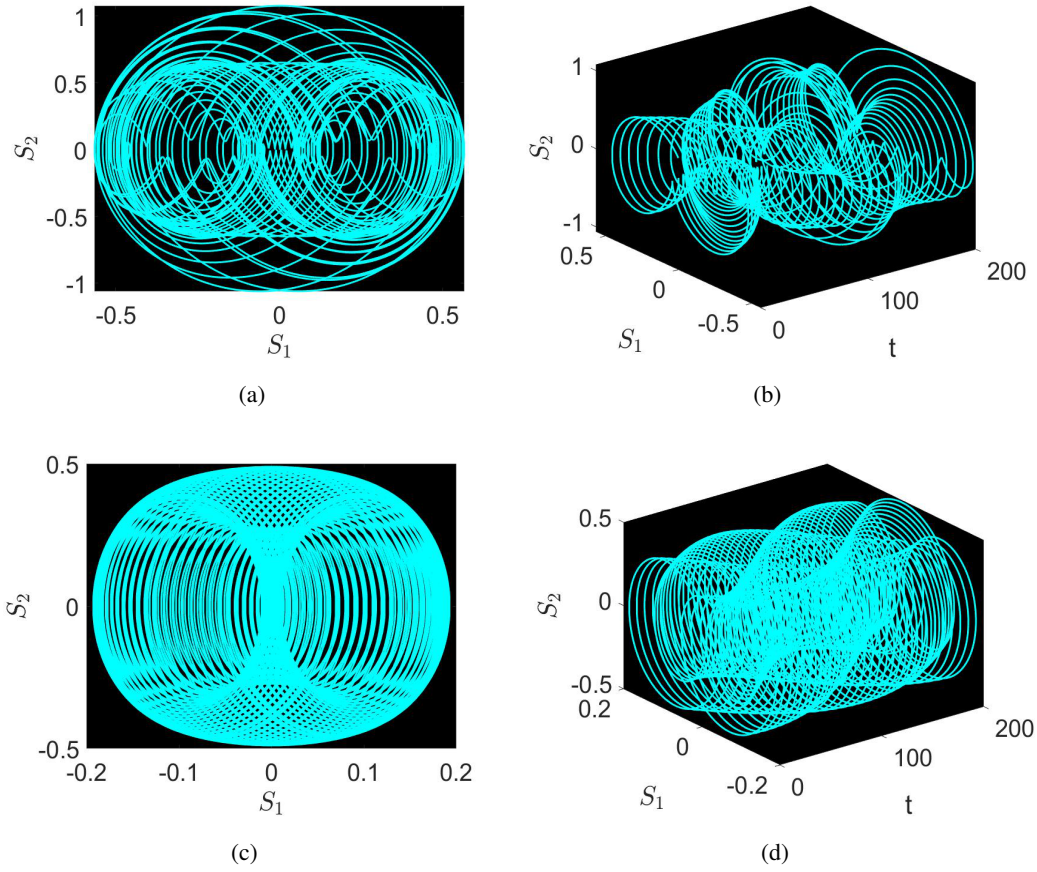

Figure 7. Using random parametric parameters, the system's chaotic behavior in two and three dimensions is physically visualized (5.3).

6. Sensitivity analysis

In this part, we elaborate the sensitivitive analysis [32] of the model described in Eq (5.3). The comparison and review of the two and three solutions are shown in Figures 8 and 9, with varying parameter values $\gamma = 0.74$, $\lambda = 0.91$, $\alpha = -0.2$ respectively. The plots demonstrate the evolution of the system's variable S_1 with regard to S_2 under various initial conditions. Figure 8 shows two types of solutions: $(S_1, S_2) = (0.6, 0)$ in red and $(S_1, S_2) = (0, .6)$ in yellow. It shows how sensitive the system is to initial conditions, as evidenced by the various oscillatory behaviors it displays over time. Similarly, Figure 9 shows three solutions: $(S_1, S_2) = (0.49, 0)$ in yellow and $(S_1, S_2) = (0, 0.7)$ in

cyan line, $(S_1, S_2) = (0.79, 0.79)$ in red. All three trajectories evolve differently despite starting from close but different points, which supports the existence of chaotic dynamics in the system. Sensitivity analysis of dynamical models is necessary to simplify complexity, ensure stability, identify crucial parameters, optimize performance, validate models, and inform management and policy choices. It is also necessary to understand how systems behave over time. It is a crucial instrument for managing the intricacies and unpredictability present in time-dependent systems.

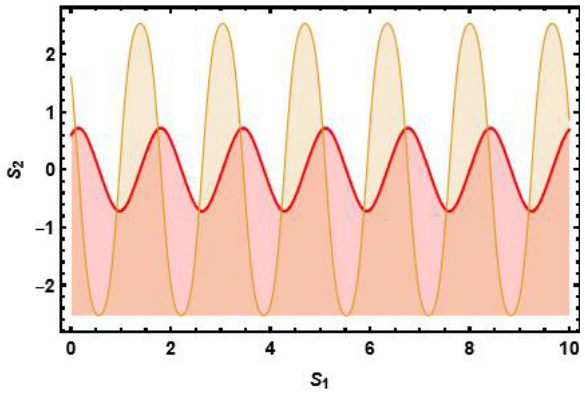

Figure 8. Analysis of sensitivity for the initial conditions in a controlled system (5.3) $(S_1, S_2) = (0.6, 0)$ in red and $(S_1, S_2) = (0, .6)$ in yellow.

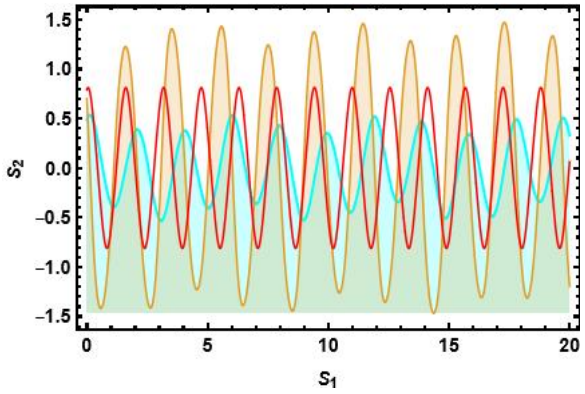

Figure 9. Analysis of sensitivity for the initial conditions in a controlled system (5.3) $(S_1, S_2) = (0.49, 0)$ in yellow, $(S_1, S_2) = (0, 0.7)$ in cyan and $(S_1, S_2) = (0.79, 0.79)$ in red.

7. Result and discussion

In this part, the novelty and originality of the current study is demonstrated by a comprehensive comparison with previous result. In a previous study, the author Chen et. al [28] established two analytical techniques to obtain exact solutions of the above mentioned model. In contrast, our research provides a more extensive examination by employing a multifaceted analysis, encompassing Lie symmetry analysis, bifurcation analysis, and sensitivity analysis. The differential equations of the Ivancevic system are first made simpler through the application of Lie symmetry analysis. PDEs are made simpler into ODEs by continuous symmetries found by Lie analysis. Finally, the Paul-Painlevé

scheme is applied to find the exact solutions of these ODEs. With certain symmetry, the model produces closed-form solutions for option prices. Moreover, we utilized the analysis for bifurcation of the aforementioned problem to enhance the understanding of the associated planar dynamical model. The analysis shows that the dynamical model deviates from anticipated trends when an external periodic disturbance term is involved. The analysis of sensitivity for the governed model was thoroughly analyzed at various initial conditions. The comprehensiveness of our research, which compares the quantitative soundness of different methodologies, is our distinctive contribution. With our collection of solutions and graphical depictions, we offer a greater understanding of the nonlinear dynamics and wave characteristics contained in the Ivancevic option pricing model. With their combination of theoretical depth and real-world application, the related methodologies mark a substantial achievement in the field of financial economics. Here we offer 3D, 2D, and contour visualizations illustrating the obtained results, emphasizing the physical significance of the considered model. Visual aids provide additional insight into the physical characteristics and nonlinear behavior of the chosen system. Three-dimensional plots are used to demonstrate the magnitude and form of solitary waves, two-dimensional plots are used to evaluate the analytical solutions' accuracy and coherence. Careful considerations was given by choosing the appropriate parameter values in the creation of these graphic representations. The periodic invariant solution of Eq (4.8) has a clear graphical structure, as shown in Figure 1. Similarly, Figure 2 illustrates the hyperbolic solution of Eq (4.13). Phase variation plots with arbitrary parameters and no perturbation term are shown in Figures 3–5. Figures 6 and 7, illustrate the 3D and 2D chaotic flows of the dynamical model (5.3) using different appropriate parameters. Figures 8 and 9, elaborates the graphical prescription of sensitivity analysis of the above mentioned model using different initial conditions. The relatively arbitrary choice of model parameters, which could affect the generalizability and robustness of our conclusions, is one of the study's limitations. The selected numbers might not accurately represent actual market dynamics, even though they show how the Ivancevic model behaves theoretically. Future studies should examine the sensitivity and logic of parameter selection, especially in light of important variables like option maturity, interest rates, and market volatility. The model may be adjusted for various assets and market conditions using parameter calibration techniques, such as optimization based on past market data or Bayesian inference methods.

8. Conclusions

In this research, we systematically examine the Ivancevic option pricing model, which incorporates stochastic volatility and nonlinear dynamics, marking a major breakthrough in the field of financial economics. This research has been conducted from a variety of vantage points, including Lie symmetry, invariant solutions, bifurcation, and sensitivity analysis. We explored the infinitesimal generators of the Ivancevic option pricing model, which have been used to construct the most efficient system of subalgebras. Moreover, we compute the point symmetry reductions on the vector fields that make up an optimum system. Following the transformation of the PDE to a few ODEs through symmetry reduction, the specific exact solutions of these ODEs are subsequently extracted using the Paul-Painlevé method. Furthermore, we investigated the bifurcation analysis of the selected model with the aid of bifurcation theory principles. Also, a comprehensive sensitivity analysis of the governed model has been thoroughly analyzed at various initial conditions. These results provide an

important new understanding of the nonlinear features of the model and establish the structure for future studies in soliton dynamics and nonlinear occurrences in related systems. The innovative approaches evaluated here may apply to many different nonlinear models, providing valuable insights into their dynamics.

Use of Generative-AI tools declaration

The authors declare that they have not used Artificial Intelligence (AI) tools in the creation of this article.

Acknowledgments

This work was supported and funded by the Deanship of Scientific Research at Imam Mohammad Ibn Saud Islamic University (IMSIU) (Grant Number IMSIU-DDRSP2502).

Conflict of interest

The author declares that he has no conflict of interest.

References

1. V. Kumar, R. Jiwari, A. R. Djurayevich, M. U. Khudoyberganov, Hyperbolic (3+ 1)-dimensional nonlinear Schrödinger equation: Lie symmetry analysis and modulation instability, *J. Math.*, **2022** (2022), 9050272. https://doi.org/10.1155/2022/9050272
2. Q. He, P. Xia, C. Hu, B. Li, Public Information, actual intervention, and infaation expectations, *Transform. Bus. Econom.*, **21** (2022), p644.
3. S. Akram, J. Ahmad, Dynamical behaviors of analytical and localized solutions to the generalized Bogoyavlvensky-Konopelchenko equation arising in mathematical physics, *Opt. Quant. Electron.*, **56** (2024), 380. https://doi.org/10.1007/s11082-023-05913-3
4. T. Han, H. Rezazadeh, M. U. Rahman, High-order solitary waves, fission, hybrid waves and interaction solutions in the nonlinear dissipative (2+ 1)-dimensional Zabolotskaya-Khokhlov model, *Phys. Scr.*, **99** (2024), 115212. https://doi.org/10.1088/1402-4896/ad7f04
5. P. Li, S. Shi, C. Xu, Bifurcations, chaotic behavior, sensitivity analysis and new optical solitons solutions of Sasa-Satsuma equation, *Nonlinear Dyn.*, **112** (2024), 7405–7415. https://doi.org/10.1007/s11071-024-09438-6
6. L. Kaur, A. M. Wazwaz, Optical soliton solutions of variable coefficient Biswas–Milovic (BM) model comprising Kerr law and damping effect, *Optik*, **266** (2022), 169617. https://doi.org/10.1016/j.ijleo.2022.169617
7. R. Zhang, S. Bilige, T. Chaolu, Fractal solitons, arbitrary function solutions, exact periodic wave and breathers for a nonlinear partial differential equation by using bilinear neural network method, *J. Syst. Sci. Complex.*, **34** (2021), 122–139. https://doi.org/10.1007/s11424-020-9392-5

8. L. A. AL-Essa, M. ur Rahman, Analysis of Lie symmetry, bifurcations with phase portraits, sensitivity and diverse W-M-shape soliton solutions for the (2+1)-dimensional evolution equation, *Phys. Letters A*, **525** (2024), 129928. https://doi.org/10.1016/j.physleta.2024.129928

9. G. Akram, M. Sadaf, M. Khan, H. Hosseinzadeh, Analytical solutions of the fractional complex ginzburg-landau model using generalized exponential rational function method with two different nonlinearities, *Adv. Math. Phys.*, **2023** (2023), 9720612. https://doi.org/10.1155/2023/9720612

10. M. Gaballah, R. M. El-Shiekh, L. Akinyemi, H. Rezazadeh, Novel periodic and optical soliton solutions for Davey-Stewartson system by generalized Jacobi elliptic expansion method, *Int. J. Nonlinear Sci. Numer. Simul.*, **24** (2024), 2889–2897.

11. T. Furuya, P. Z. Kow, J. N. Wang, Consistency of the Bayes method for the inverse scattering problem, *Inverse Probl.*, **40** (2024), 055001. https://doi.org/10.1088/1361-6420/ad3089

12. T. Yin, Z. Xing, J. Pang, Modified Hirota bilinear method to (3+1)-D variable coefficients generalized shallow water wave equation, *Nonlinear Dyn.*, **111** (2023), 9741–9752. https://doi.org/10.1007/s11071-023-08356-3

13. Y. Wang, X. Lü, Bäcklund transformation and interaction solutions of a generalized Kadomtsev–Petviashvili equation with variable coefficients, *Chinese J. Phys.*, **89** (2024), 37–45. https://doi.org/10.1016/j.cjph.2023.10.046

14. M. A. El-Shorbagy, S. Akram, M. ur Rahman, Propagation of solitary wave solutions to (4+1)-dimensional Davey-Stewartson-Kadomtsev-Petviashvili equation arise in mathematical physics and stability analysis, *PDE Appl. Math.*, **10** (2024), 100669. https://doi.org/10.1016/j.padiff.2024.100669

15. S. Yadav, M. Singh, S. Singh, S. Heinrich, J. Kumar, Modified variational iteration method and its convergence analysis for solving nonlinear aggregation population balance equation, *Comput. Fluids*, **274** (2024), 106233. https://doi.org/10.1016/j.compfluid.2024.106233

16. A. R. Seadawy, M. Iqbal, D. Lu, Propagation of kink and anti-kink wave solitons for the nonlinear damped modified Korteweg-de Vries equation arising in ion-acoustic wave in an unmagnetized collisional dusty plasma, *Phys. A: Stat. Mech. Appl.*, **544** (2020), 123560. https://doi.org/10.1016/j.physa.2019.123560

17. Z. Eskandari, Z. Avazzadeh, R. Khoshsiar Ghaziani, B. Li, Dynamics and bifurcations of a discrete-time Lotka-Volterra model using nonstandard finite difference discretization method, *Math. Meth. Appl. Sci.*, 2022. https://doi.org/10.1002/mma.8859

18. J. Pan, M. U. Rahman, Rafiullah, Breather-like, singular, periodic, interaction of singular and periodic solitons, and a-periodic solitons of third-order nonlinear Schrödinger equation with an efficient algorithm, *Eur. Phys. J. Plus*, **138** (2023), 912. https://doi.org/10.1140/epjp/s13360-023-04530-z

19. X. Zhu, P. Xia, Q. He, Z. Ni, L. Ni, Ensemble classifier design based on perturbation binary salp swarm algorithm for classification, *CMES-Comput. Model. Eng. Sci.*, **135** (2023), p653. https://doi.org/10.32604/cmes.2022.022985

20. F. Black, M. Scholes, The pricing of options and corporate liabilities, *J. Polit. Economy*, **81** (1973), 637–654.

21. B. E. Baaquie, A path integral approach to option pricing with stochastic volatility: some exact results, *J. Phys. I*, **7** (1997), 1733–1753. https://doi.org/10.1051/jp1:1997167

22. E. Haven, An *h*-Brownian motion'and the existence of stochastic option prices, *Phys. A: Stat. Mech. Appl.*, **344** (2004), 152–155. https://doi.org/10.1016/j.physa.2004.06.107

23. Y. Q. Chen, Y. H. Tang, J. Manafian, H. Rezazadeh, M. S. Osman, Dark wave, rogue wave and perturbation solutions of Ivancevic option pricing model, *Nonlinear Dyn.*, **105** (2021), 2539–2548. https://doi.org/10.1007/s11071-021-06642-6

24. R. M. Jena, S. Chakraverty, D. Baleanu, A novel analytical technique for the solution of time-fractional Ivancevic option pricing model, *Phys. A: Stat. Mech. Appl.*, **550** (2020), 124380. https://doi.org/10.1016/j.physa.2020.124380

25. Z. Yan, Vector financial rogue waves, *Phys. Letters A*, **375** (2011), 4274–4279. https://doi.org/10.1016/j.physleta.2011.09.026

26. S. O. Edeki, O. O. Ugbebor, O. González-Gaxiola, Analytical solutions of the Ivancevic option pricing model with a nonzero adaptive market potential, *Int. J. Pure Appl. Math.*, **115** (2017), 187–198. https://doi.org/10.12732/ijpam.v115i1.14

27. V. G. Ivancevic, Adaptive-wave alternative for the Black-Scholes option pricing model, *Cogn. Comput.*, **2** (2010), 17–30. https://doi.org/10.1007/s12559-009-9031-x

28. Q. Chen, H. M. Baskonus, W. Gao, E. Ilhan, Soliton theory and modulation instability analysis: The Ivancevic option pricing model in economy, *Alex. Eng. J.*, **61** (2022), 7843–7851. https://doi.org/10.1016/j.aej.2022.01.029

29. B. Li, Y. Zhang, X. Li, Z. Eskandari, Q. He, Bifurcation analysis and complex dynamics of a Kopel triopoly model, *J. Comput. Appl. Math.*, **426** (2023), 115089. https://doi.org/10.1016/j.cam.2023.115089

30. T. Mahmood, G. Alhawael, S. Akram, M. ur Rahman, Exploring the Lie symmetries, conservation laws, bifurcation analysis and dynamical waveform patterns of diverse exact solution to the Klein–Gordan equation, *Opt. Quant. Electron.*, **56** (2024), 1978. https://doi.org/10.1007/s11082-024-07814-5

31. M. A. El-Shorbagy, S. Akram, M. ur Rahman, H. A. Nabwey, Analysis of bifurcation, chaotic structures, lump and $M-W$-shape soliton solutions to (2+1) complex modified Korteweg-de-Vries system, *AIMS Math.*, **9** (2024), 16116–16145. http://dx.doi.org/10.3934/math.2024780

32. A. M. Alqahtani, S. Akram, J. Ahmad, K. A. Aldwoah, M. ur Rahman, Stochastic wave solutions of fractional Radhakrishnan–Kundu–Lakshmanan equation arising in optical fibers with their sensitivity analysis, *J. Opt.*, 2024. https://doi.org/10.1007/s12596-024-01850-w